Radiation damage buildup and dislocation evolution in Ni and equiatomic multicomponent Ni-based alloys

E. Levo[a], F. Granberg[a], C. Fridlund[a], K. Nordlund[a], F. Djurabekova[a,b]

[a] *Department of Physics, P.O Box 43, FIN-00014, University of Helsinki*
[b] *Helsinki Institute of Physics, P.O. Box 43, FIN-00014, University of Helsinki*

Abstract

Single-phase multicomponent alloys of equal atomic concentrations ("equiatomic") have proven to exhibit promising mechanical and corrosion resistance properties, that are sought after in materials intended for use in hazardous environments like next-generation nuclear reactors. In this article, we investigate the damage production and dislocation mobility by simulating irradiation of elemental Ni and the alloys NiCo, NiCoCr, NiCoFe and NiFe, to assess the effect of elemental composition. We compare the defect production and the evolution of dislocation networks in the simulation cells of two different sizes, for all five studied alloys. We find that the trends in defect evolution are in good agreement between the different cell sizes. The damage is generally reduced with increased alloy complexity, and the dislocation evolution is specific to each material, depending on its complexity. We show that increasing complexity of the alloys does not always lead to decreased susceptibility to damage accumulation under irradiation. We show that, for instance, NiCo alloy behaves very similarly to Ni, while presence of Fe or Cr in the alloy even as a third component reduces the saturated level of damage substantially. Moreover, we linked the defect evolution with the dislocation transformations in the alloys. Sudden drops in defect number and large defect fluctuations from the continuous irradiation can be explained from the dislocation activity.

Keywords: Radiation, damage, equiatomic, multicomponent, alloy

1. Introduction

The ever-increasing demand for energy requires developing new concepts of energy production, that will produce electricity more efficiently and in a more environmentally friendly manner. Development of future energy production concepts have led to a demand of new materials able to operate in extreme conditions. The search for materials with high tolerance for radiation, specific

Email address: fredric.granberg@helsinki.fi (F. Granberg)

Preprint of article published by Elsevier in Journal of Nuclear Materials 490 (2017) 323-332

mechanical properties and good corrosion resistance properties has led to increasing research of High Entropy Alloys (HEA) [1, 2, 3, 4, 5]. These alloys are a random distribution of atoms of large atomic fractions of five different elements or more. Equiatomic multicomponent (EAMC) alloys are related to the HEA family, but the number of different materials is less than in HEA and the fractions of the different elements are equal.

It has been shown that both HEA and EAMC alloys exhibit promising mechanical properties [4, 3, 6, 7, 8, 9, 10], good wear and corrosion resistance [4] and resistance to softening. Furthermore, they have shown thermal stability and hardness at high temperatures as well as good tensile strength at low temperatures [6, 7, 8]. Moreover, the same HEA's have proven to have improved fatigue, fracture resistance, ductility and strength [3, 10, 9]. Studies have also shown that the EAMC alloys have a reduced defect accumulation when exposed to continuous irradiation [5, 11, 12] and that one contributing factor for this phenomenon was reduced dislocation mobility [5, 13]. Both the experimental and simulation efforts showed that NiFe and NiCoCr have a tendency of less accumulating defects in massively overlapping cascades [5] compared to elemental Ni. The experimental work demonstrated, and the simulations indicated, a clear difference between the two alloys, where NiCoCr showed an even larger reduction in accumulated defects [5]. The previous investigations proved that the dislocation mobility clearly differs for the different materials, where Ni has the highest and NiCoCr the lowest [5, 13]. The lower dislocation mobility in the more complex alloys prevents a rapid formation of large dislocation structures, leading to a smaller amount of prevailing defects.

In the last decades, computer simulations have been proven to be an advantageous supplement to experiments. Computer simulations can be used to study the atomistic evolution of materials in real time. In the case of irradiation, computer simulations, especially Molecular Dynamics (MD) simulations, are able to reproduce the time evolution of primary damage production during irradiation [14, 15, 16]. In this article, we present data on the defect production from MD simulations of irradiation of several different EAMC alloys of different complexity.

A previous study [5] investigated the defect accumulation in pure Ni and compared it with the NiFe- and NiCoCr alloys, in simulation cells containing 108 000 atoms. In this article, we focus on a larger cell, containing 500 000 atoms, to study the possible finite size effects and to obtain even more detailed results, on the damage production. In addition to NiFe and NiCoCr we simulated the radiation effects in two other alloys, NiCo and NiCoFe, to investigate whether the choice of alloying elements affects the results. Along with the damage accumulation in the different alloys, we throroughly investigated the accumulation of dislocations as well as their evolution in the samples. We also determined the effect of the dislocation evolution on the retained defect amount and defect behavior. To enable a systematic study of all five materials, we ran the simulations for the previous system [5] with the new alloys. We analyzed the mobility of edge dislocations in NiCo and NiCoFe, and compared it to the previous results [13].

2. Methods

2.1. MD Simulations

In the paper by Granberg *et al.* [5] damage evolution results for Ni, NiFe and NiCoFe were presented from simulation cells comprising 108 000 atoms, hereafter referred to as the small cell. In order to reinforce these results, we ran similar simulations for cells comprising 500 000 atoms, hereafter referred to as the large cell, and with a cell size of about $180 \times 180 \times 180$ Å^3 to 0.34 dpa [17]. In addition to this, we also simulated both small and large cells for two other compositions, NiCo and NiCoFe, to investigate the effect of the nature of alloying components.

For the recoil simulations, we utilized the classical MD code PARCAS [18, 19]. The EAM potentials used to describe the atomic interactions in our cells were those of Zhou *et al.* [20] and Lin *et al.* [21]. The potential by Zhou *et al.* was used to describe Ni, NiCo, NiCoFe and NiFe, while a combination of the NiCo potential by Zhou *et al.* and the Cr potential by Lin *et al.* was used to describe NiCoCr. We also used an electronic stopping power [22] and the ZBL repulsive potential [23], joining it smoothly together with all the equilibrium potentials, in order to handle the high energy effects in the collision cascades. The five materials of different compositions, Ni, NiCo, NiCoCr, NiCoFe and NiFe, were simulated for 4 000 cascade events for the large cell, resulting in a dose of 0.344 dpa, and 1 500 cascades events for the small cells, resulting in 0.57 dpa. A threshold displacement energy of 40 eV has been used for all materials to be consistent with the values used in previous experiments [5]. Each event consisted of a 5 keV recoil followed by a relaxation period, during which the system temperature was cooled down to about 300 K. Each event lasted for 30 ps.

We controlled the temperature by applying Berendsen temperature control [24] on the atoms found within a 0.4 nm thick layer at all sides of the cell. These atoms are identified only by their positions and thus redefined before every recoil event. This was done during the simulations of atomic cascades to avoid the self-heating of the cell due to the periodic boundary condition. In order to prevent the recoil atoms from reaching the temperature controlled border atoms, all recoils were initialized at the centre of the simulation cell. To simulate random impact positions of initial recoils for a homogeneous irradiation effect, we shifted the cell before each recoil event by a vector of random magnitude (not greater than the cell size) and direction. After this shift, atoms outside the cell boundaries were shifted back using periodic boundary conditions. The simulations of all elemental compositions were repeated three times, with different random seeds, in order to produce a mean trend for the damage production in the cells and to show that it does not depend on stochastic anomalies.

We also ran 100 cases of single impact cascades for each material, with the same 5 keV recoil energy. For these simulations, we created the initial cell states for the different cases by shifting one relaxed cell. We ran the single

Colour	Burger's Vector	Name
Dark Blue	$1/2\langle 1\,1\,0\rangle$	Perfect
Green	$1/6\langle 1\,1\,2\rangle$	Shockley
Purple	$1/6\langle 1\,1\,0\rangle$	Stair-rod
Yellow	$1/3\langle 0\,0\,1\rangle$	Hirth
Light Blue	$1/3\langle 1\,1\,1\rangle$	Frank
Red	-	Other

Table 1: The dislocation color in the movies and their corresponding Burgers vectors and names.

impact cascades to describe and analyze the very early stage of defect evolution in EAMC alloys due to the overlapping cascades.

For each composition of the studied alloys, we investigated the mobility of perfect $1/2\langle 1\,1\,0\rangle$ edge dislocations at room temperature in three randomly constructed cells, to obtain the stochastical differences. The dislocation behaviour was investigated at different constant shear stresses, to obtain the stress dependent dislocation velocity. The edge dislocation mobility in NiCo and NiCoFe was obtained following exactly the same method as in Ref. 13, where the edge dislocation mobility in Ni, NiFe and NiCoCr is described.

2.2. Damage Analysis

For the point-defect analysis we used the Wigner-Seitz cell method [18], to determine the number of vacancies and interstitials in the samples. In the following, we also use the numbers of defects, including both vacancies and interstitials, to compare the level of damage in different simulation cells. The defect concentration is the number of these defects per atom. In the case of single impact damage, we studied 100 different impacts to obtain the average defect productions in the different alloys. The same method was used for the overlapping cascade simulations, where the results given are the averages of three different simulation series.

We analyzed the existing dislocations in the cells with the Open Visualization Tool OVITO [25] and the dislocation extraction algorithm (DXA) [26] implemented in it. Examples of defect structures obtained with the DXA analysis are shown in Figs. 1 and 2, where the different colored lines represents different dislocation types, listed in Table 1, and the volumes represent defect clusters. We present in the Supplementary material, in addition to the quantitative analysis of the evolution of damage production in the studied alloys, movies illustrating the evolution of dislocation networks in all the investigated alloys.

3. Results and Discussion

The Results and Discussion section is structured as follows: In subsection 3.1, the evolution of damage production in terms of point defects is analyzed in the

cells of both studied sizes as a function of accumulated dose. Also a comparison with the single impact results is presented. In subsection 3.2, the detailed analysis of the dislocation network is presented for all simulation cells, and the link between the dislocation evolution and the fluctuations of the actual amount of the defects in the cells is discussed. In subsection 3.3, the dislocation mobility for edge dislocations is presented, in the two materials (NiCo and NiCoFe) not studied previously. All results in the graphs are the averages over three different simulation runs, unless specified differently.

Some of the results from Refs. 5 and 13 are added to the current results to enable the comparative study for all five compositions. In Ref. 5, the defect concentration as a function of dose is given for Ni, NiFe and NiCoCr for the small 108 000 atom cell up to 0.3 dpa. These results were extended to the dose of 0.57 dpa (1 500 recoils) in order to analyze the radiation tolerance of EAMC alloys at even higher doses than studied earlier. Moreover, in this article we investigate the dislocation mobility in two new alloys, NiCo and NiCoFe, and compare the results to those from Ref. 13.

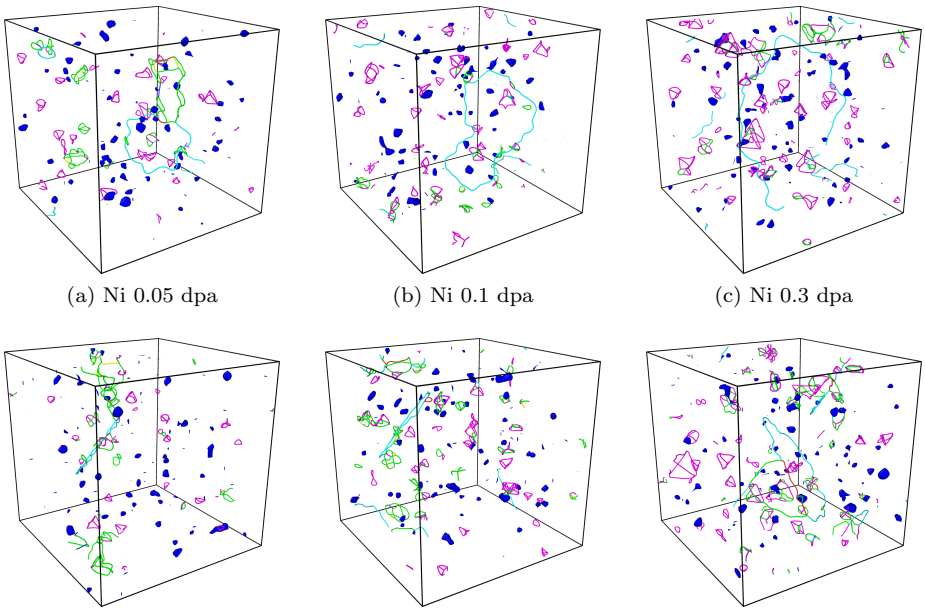

(a) Ni 0.05 dpa (b) Ni 0.1 dpa (c) Ni 0.3 dpa

(d) NiCo 0.05 dpa (e) NiCo 0.1 dpa (f) NiCo 0.3 dpa

Figure 1: Snapshots of the dislocation networks and defect clusters in Ni and NiCo, at the doses 0.05, 0.1 and 0.3 dpa. The length of all sides are 50 unitcells, $\sim$ 18 nm. The lines of different color represents dislocations with different Burgers vectors, where green is a Shockley, purple a stair-rod, light blue a Frank, yellow a Hirth and dark blue a perfect dislocation. The dark blue volumes represents defect clusters.

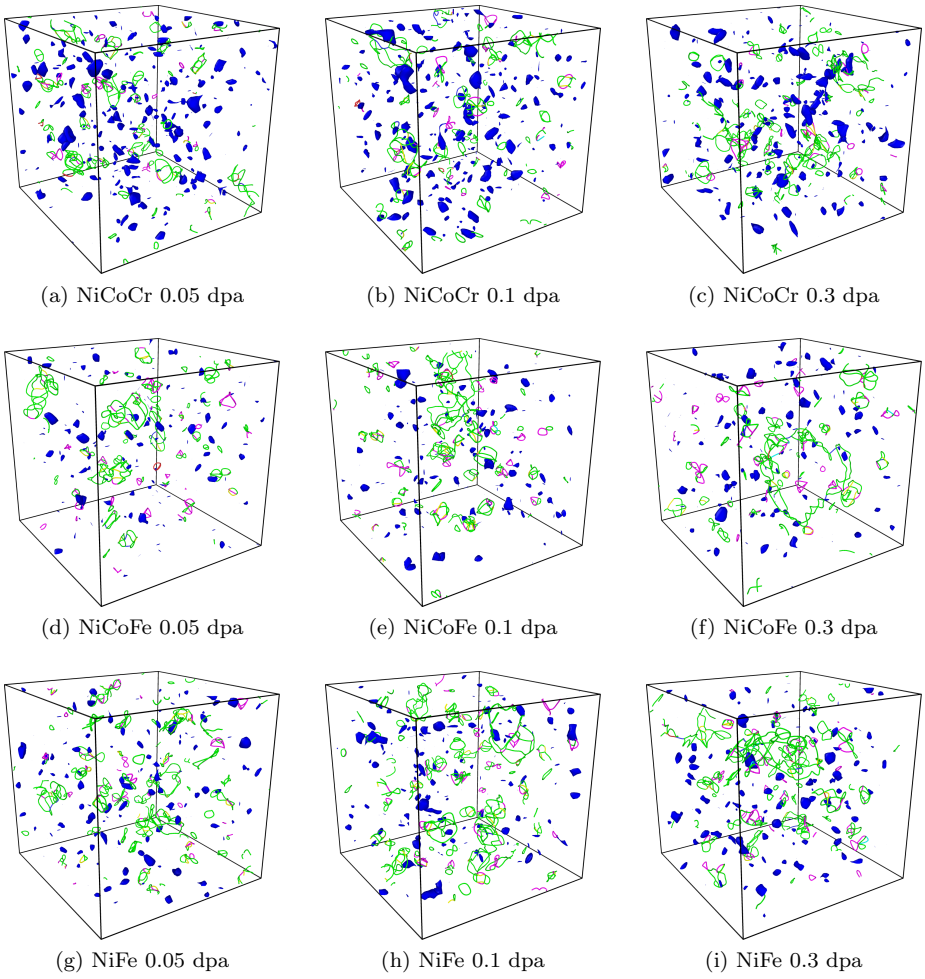

(a) NiCoCr 0.05 dpa (b) NiCoCr 0.1 dpa (c) NiCoCr 0.3 dpa

(d) NiCoFe 0.05 dpa (e) NiCoFe 0.1 dpa (f) NiCoFe 0.3 dpa

(g) NiFe 0.05 dpa (h) NiFe 0.1 dpa (i) NiFe 0.3 dpa

Figure 2: Snapshots of the dislocation networks and defect clusters in NiCoCr, NiCoFe and NiFe, at the doses 0.05, 0.1 and 0.3 dpa. The length of all sides are 50 unitcells, $\sim$ 18 nm. The meaning of the lines are the same as in Fig. 1.

3.1. Defect Build-up

In Fig. 3, the defect data between the small (Fig. 3a) and the large (Fig. 3b) cells, are compared for all materials investigated. In Fig. 3a, we see that the same trend previously seen in Ref. 5, extends up to 0.57 dpa. The number of defects are highest in Ni, while both NiFe and NiCoCr results in lower, but similar number of defects. When the two new alloys, NiCo and NiCoFe, are added, we clearly see the difference between them. NiCo behaves very similarly to pure Ni, and NiCoFe shows similar behaviour as NiFe and NiCoCr. If we compare the defect number in the small cell (Fig. 3a) and the large cell (Fig. 3b), we see

a similar trend. The defect number is again highest in Ni. The main difference, however, is that NiFe, NiCoFe and NiCoCr do not follow the same behavior as in Fig. 3a. Instead, the number of defects is higher in NiFe than in NiCoFe, and NiCoCr has clearly the lowest number of defects. This separation and this order of highest to lowest number of defects, was also seen experimentally [5, 27] (except for NiCoFe).

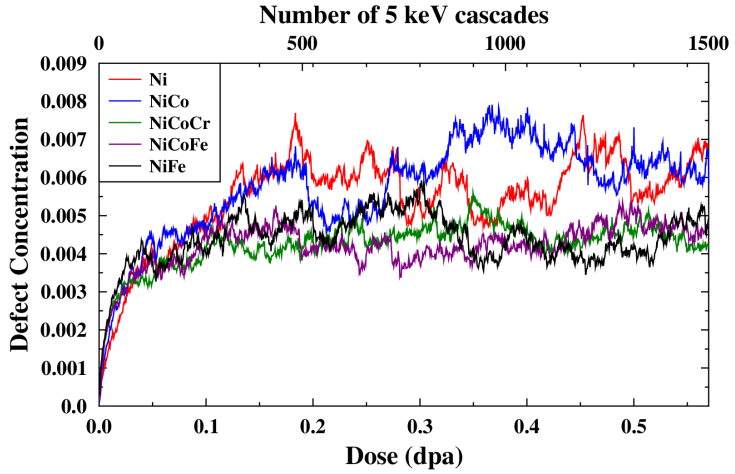

(a) 108 000 atom cell

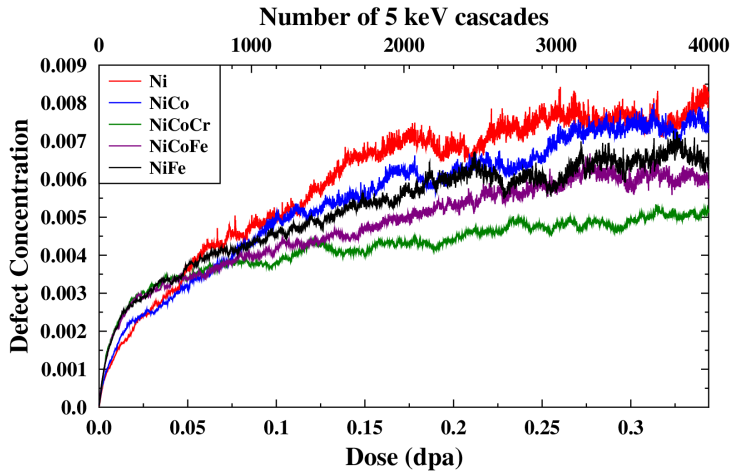

(b) 500 000 atom cell

Figure 3: Comparison of defect concentration evolution in the (a) 108 000 atom cell and (b) 500 000 atom cell.

Figs. 3a and 3b indicate that the addition of an element is not enough to

obtain the lower defect accumulation, if we compare pure Ni with the two two-element EAMC-alloys. Both figures clearly show that the addition of Co to the Ni structure did not affect the saturation level of the defects, whereas the presence of Fe lowered the defect saturation level substantially in both NiCoFe and NiFe. One explanation could be that the dislocation mobilities in Ni and NiCo are very similar [5, 13] due to similar close-packed crystal structures (Ni has natively FCC and Co has HCP), while the presence of Fe (natively in a BCC lattice) disturbs the atomic arrangement much more, which is reflected in the dislocation mobility in the alloys containing Fe. The results also indicate that already 33 percent of Fe (randomly distributed in the cell) is enough to obtain a lower defect accumulation, in the investigated crystal structure. Comparison of the behavior of the NiCoFe and NiFe alloys with NiCoCr alloys shows very similar trend in the small cell, while in the large cell we see a clear decrease of the defect saturation level in NiCoCr, compared to the cells containing Fe.

The size evolution of defect clusters is also seen to vary in the different materials. We can see from Figs. 1 and 2 as well as in the dislocation movies (described later in more detail) that the dislocation structures form and grow more quickly in Ni and NiCo than the rest of the materials. Small defect clusters are created in NiFe, NiCoFe and NiCoCr and grow slowly, but are able to combine later on to form clusters of significant sizes.

In both the small and large simulation cells, we observe in the beginning that the number of defects is higher in the more complex alloys, compared to Ni and NiCo [13]. This is seen as a faster accumulation of defects in NiFe, NiCoFe and NiCoCr compared to Ni and NiCo in the interval up to 0.03 - 0.05 dpa. In the large cell there is a clear difference in the behavior of the damage growth curves when comparing Ni and NiCo with the other alloys, whereas in the small cell a similar difference can also be seen, but much less evidently. (See Supplementary for a zoom in of the beginning of Fig. 3). This is in contradiction to the higher dose results, where the number of accumulated defects is much lower in the alloys, which show a faster growth in the beginning.

To analyze in more detail what happens in the beginning of the overlapping cascade simulations, we ran single impacts in the different materials. The results for 100 single impact cascades can be seen in Table 2, where the average number of point defects produced by a single 5 keV recoil is given. From the results we see that the amount of primary damage is a bit higher in the complex alloys compared to Ni and NiCo, which can explain the behaviour in the low dose regime. The difference between Ni and NiCo compared to the other alloys in the plotted data in Fig. 3b is similar to the data in Table 2 in the low dose regime. In the beginning, upto a dose of 0.0025 dpa the defect concentration is increasing linearly and the difference between Ni and NiCo compared to the other alloys can be explained by the number of defects produced in a single cascade. Previous computational studies on defect production in Ni and NiFe show the same difference in the number of produced defects at a higher energy [28] This phenomenon can be explained with the greater probability of vacancy creation, during the recrystallization phase of a heat spike, in the more complex alloys [13, 29, 15]. In the single cascade events, we see that in a few

cases stacking fault tetrahedra (SFT) are formed, but very rarely, due to the low energy and low number of vacancies that could create a SFT. In 5% to 10% of the cascades also stair-rod loops were formed. But in addition to the number of point defects created, we can see a difference in the number of Shockley partial loops formed (and recognized by OVITO). They were observed in Ni and NiCo in $\sim 10\%$ of the cascades, whereas in the other alloys they were observed in 30% to 50% of the cases. All the formed defect structures were small in size, due to the very low amount of created point defects. Some of the curious developments in defect evolution, like sudden defect drops, will be discussed in more detail in the subsection 3.2, and the dislocation mobilities are discussed later in this article.

Alloy	Defect amount
Ni	16.22 ± 0.71
NiCo	16.72 ± 0.72
NiCoCr	21.54 ± 0.74
NiCoFe	19.68 ± 0.75
NiFe	21.80 ± 0.79

Table 2: Amount of vacancies and interstitials produced by a single 5 keV cascade. The numbers are averages over 100 independent events. The error bars are the standard error of the mean.

From the defect accumulation investigation we can conclude that we can qualitatively obtain similar results in the smaller cells as in the larger cells. The same trends, defect accumulation in the beginning, defect saturation levels and the material order, were seen in both cell sizes. Some differences are also seen, mainly the stochastic fluctuations are much more dramatic in the small cells, which can be explained by the fact that the destruction of a single defect cluster will have a bigger impact on the total defect concentration in smaller cells than in larger cells. Another difference seen is the defect saturation level and how fast it is achieved. The saturation is achieved faster and at lower number of defects, is in the small cell is mainly due to the finite size effect. In the large cell the dislocations grow larger than in the small cell, before they start actively intersecting with each other and overlapping with the atomic cascades, reducing the damage buildup rate. We validated our model in [30], where the cells of one of the irradiated EAMC from consecutive MD runs were used to simulate the Rutherford Backscattering spectra in channeling mode (RBS-C). The good comparison of these results with experiment confirms the adequacy of the model and that the MD simulations here are representative of the experimental setup.

3.2. Dislocation Structures and Evolution

In the study of the dislocation structures at different doses, we focused on the evolution in the large cells. We noticed that the trends are similar in the small and large cells, but the large stochastic fluctuations render the results of the small cells inferior for analysis compared to the results of the large cells.

In our dislocation analysis, the main focus is on Frank loops, Shockley partial chains, Shockley loops, stair-rod loops and Stacking Fault Tetrahedra (SFT). The number of SFTs is obtained by dividing the total amount of stair-rod segments by six. The resulting amount of SFTs is indicative, since not all stair-rod dislocations are part of an SFT. Because the amount of stair-rod dislocations becomes significantly higher when SFTs are present in a cell, this indicative result will be sufficient for a qualitative comparison of materials with a high amount of SFTs to materials with a small amount of SFTs. Differences in the defect nature and number of SFTs are evident in Figs. 1 and 2. Fig. 4 shows a graphical representation of the mean concentration of SFTs in the large cells of the different materials. We can clearly see a higher SFT concentration in Ni and NiCo, compared to NiCoCr, NiCoFe and NiFe. In the figure we can see in the beginning that the concentration of SFTs are growing in the same phase in all investigated materials. This can be seen in the Figs. 1 and 2, at the lowest dose in the different materials. Even though the concentration of SFTs according to Fig. 4 should be equal, we see in Ni and NiCo perfect SFTs whereas in the other alloys we mainly see Stair-rod loops or Stair-rod segments. At the higher doses, we see that the amount of SFTs are increasing in Ni and NiCo, but not in the other alloys, which can be seen in Figs. 1 and 2, if the two higher doses are inspected.

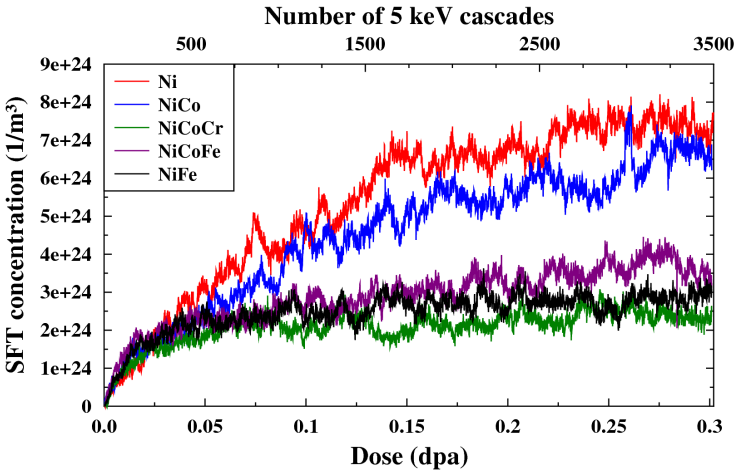

Figure 4: Comparison of the SFT concentration in the different materials (large cells).

The different materials studied showed very different tendencies to form different dislocation structures. For instance, the less complex compositions Ni and NiCo formed a couple of big Frank dislocation loops, Shockley partial chains and a multitude of SFTs that became complex (for example, two SFTs stuck to each other), see Fig. 1, and great in size later on in the simulations, while the more complex alloys NiCoCr, NiCoFe and NiFe formed mostly some small

Shockley partial chains, that were able to grow significantly given enough time, Shockley loops, some stair-rod loops and a few SFTs, see Fig. 2. Only in one of the NiCoFe cells, a significantly sized Frank loop existed for a significant time. If the results of Ni studied here is compared qualitatively with experimental observations, many similarities can be seen. Experiments show that mainly SFTs are formed, but also other small undefined defect structures as well as some large dislocations [31]. In our simulations of Ni we see that mainly SFTs are formed as well as some big dislocations (see Fig. 1a or supplementary movie of Ni). The simulations also show that smaller dislocation networks and undefined defects are formed in Ni.

We also reinforced the idea of a lower dislocation mobility in the more complex alloys, as presented in the earlier papers by Granberg *et al.* [5, 13]. We studied the dislocation movies, available in the Supplementary material, and saw that the dislocations in Ni and NiCo were quite mobile and combined with each other, resulting quickly in larger and more complex dislocation structures that were still able to move. In NiCoCr the dislocations were the least mobile, resulting in a very static dislocation evolution and a slow growth of complex dislocation structures. In NiCoFe and NiFe, the dislocations were less mobile than in Ni and NiCo but more mobile than in NiCoCr, leading to a resonable growth of complex dislocation structures that were able to, but still less likely to, move than the ones in Ni and NiCo.

By studying the dislocation movies, it became clear that there is not much interesting going on in the more complex alloys (compare Fig. 1 and Fig. 2), except in one of the NiCoFe cases. The dislocation evolution in one of the three cases of each alloy, can be seen in the Supplementary material. In the more complex alloys, there are mostly Shockley partial chains and clusters that grow slowly and recombine with each other if they happen to come close to one another. On the other hand, we saw some interesting dislocation absorption events in the less complex materials, Ni and NiCo. For instance, we noticed that a small Frank dislocation loop positioned in the vicinity of a large Shockley partial chain, eventually joined with the chain and frame by frame the whole structure converted into a complete Frank loop (see Fig. 7). We also observed an opposite phenomenon where a large Shockley partial chain absorbed a Frank loop, see Fig. 5a-c or Supplementary material: ni-a.mov 0:25-0:37. Sometimes, there was even an instantaneous transformation of a Shockley partial chain into a Frank loop, see Fig. 5d-e or Supplementary material: ni-b.mov 1:06-1:10.

Only in one of the NiCoFe cases, were we able to see an interesting absorption event between a Frank loop and Shockley partial chain. Here, a part of a Shockley partial chain transformed instantaneously into a Frank loop and persisted in the cell for a long time, until it was absorbed again by a Shockley partial chain reversing the transformation, see Fig. 6 or Supplementary material: nicofe.mov 1:30-3:47.

The phenomena of dislocation absorptions and transformations is reflected in the Wigner-Seitz analysis in two ways: by seeing significant drops in defect count during an absorption event and by being able to connect the nature of the defect count variation to the current dominating dislocation structure, *i.e.*

(a) A Shockley partial loop with a Frank loop in its vicinity, in Ni at 0.0249 dpa

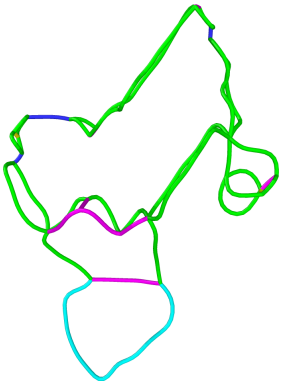

(b) The Shockley partial loop combines with the Frank loop, in Ni at 0.0267 dpa

(c) The Shockley partial chain absorbs the Frank loop completely, in Ni at 0.0318 dpa

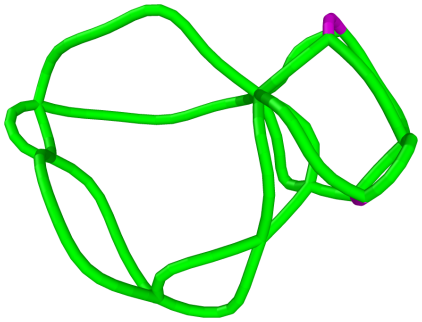

(d) The Shockley partial chain in Ni at 0.0593 dpa, before the transformation

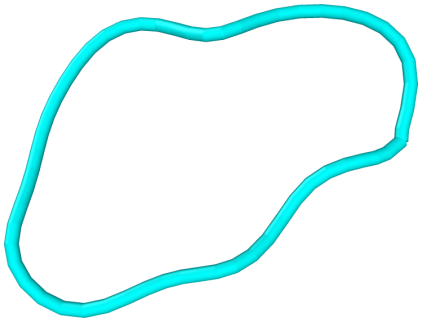

(e) The Shockley partial chain instantaneously transformes into a Frank loop at 0.0602 dpa in Ni

Figure 5: A combination of a Frank loop and a Shockley partial chain, that lead to an absorption of the Frank loop, subfigures a-c. In subfigures d and e an instantaneous transformation of a Shockley partial chain into a Frank loop. The meaning of the lines are the same as in Fig. 1.

whether it was a Frank loop or a Shockley partial chain.

If no Frank loop was there to absorb the Shockley partial chains, the defect amount would vary significantly more after each subsequent cascade, than in the presence of a Frank loop. Without the Frank loop, the Shockley partial chain would continue to grow and change in shape during the simulation. Some hybrid cases were also observed. Here, Frank loops and Shockley partial chains had mutual dominance over all other dislocations, *i.e.* they absorbed smaller dislocations but not each other (see Supplementary material: nico.mov).

We could easily divide the defect-evolution for Ni and NiCo into three dif-

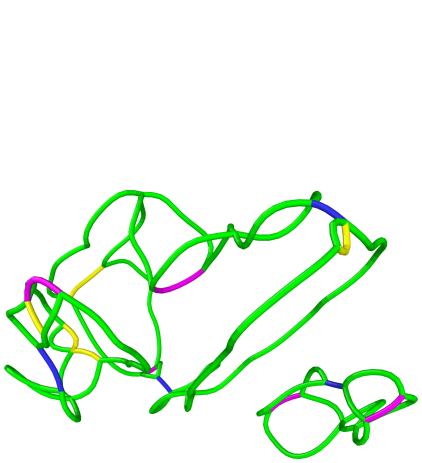

(a) An illdefined Shockley partial chain in the NiCoFe sample at 0.0774 dpa

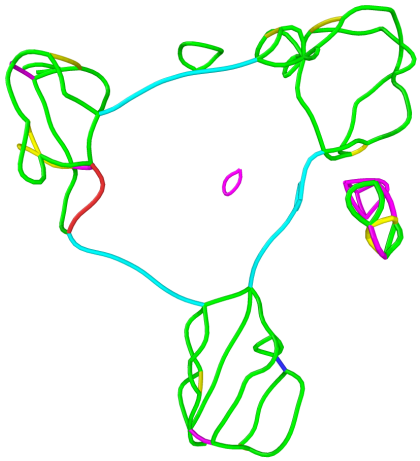

(b) A Frank loop is created at 0.1032 dpa

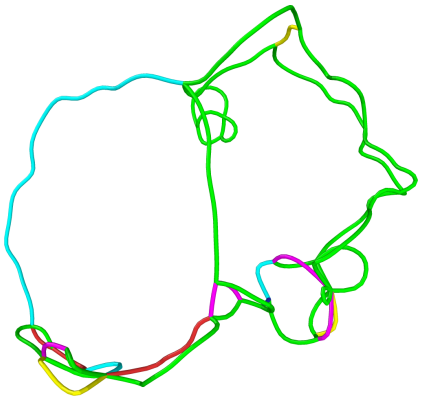

(c) The Shockley partial chain and the Frank loop are mutually existing for a long time in the cell

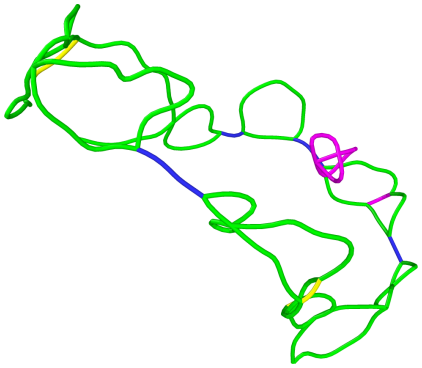

(d) The Shockley partial chain finally absorbs the Frank loop at 0.1978 dpa

Figure 6: The transformation of a Shockley partial chain into a Frank loop that exists for a long time in the NiCoFe sample. The Shockley partial chain do finally absorb the whole Frank loop. The meaning of the lines are the same as in Fig. 1.

ferent scenarios: 1) only one or more significant Frank loops were present, 2) only one or more significant Shockley partial chains were present and 3) there existed mutually dominating Frank loops and Shockley partial chains. In Fig. 7, we can see a transition from the scenario 2 to 1. Until about 0.095 dpa we can see that the defect evolution is quite turbulent. However, at about 0.095-0.1 dpa the defect count suddenly drops and the defect evolution becomes a lot

"quieter". Figs. 7b, c and d show the snapshots of the dislocations in the cell at different times. We can see a Frank loop that starts absorbing the Shockley partial chain until there is nothing left but the Frank loop.

We were able to explain the defect evolution for all the other Ni and NiCo cases in similar ways with the different scenarios by only performing the Wigner-Seitz analysis. This means that we can, to some extent, predict what dislocation structures we can see in the dislocation movies for at least Ni and NiCo, by only studying the defect evolution.

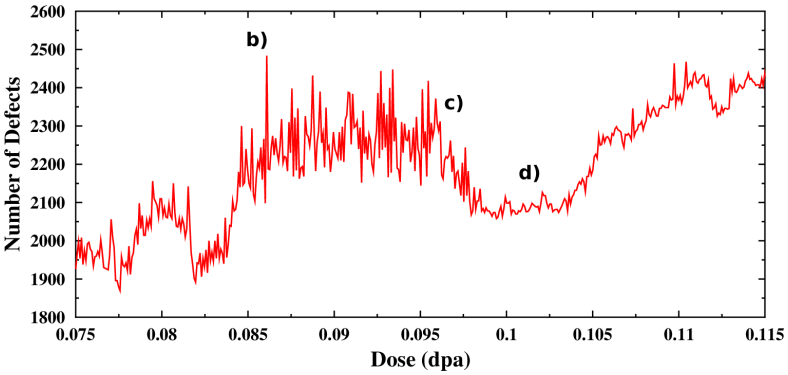

(a) Defect evolution between 0.075 dpa and 0.115 dpa and the occurences of b, c and d.

(b) At about 0.086 dpa.

(c) At about 0.097.

(d) After about 0.1 dpa.

Figure 7: Specific dislocation absorption event in large Ni (Ni-a movie in the Supplemantary manterial) cell. In subfigure a the number of defects at different doses (zoomed in at 0.075 dpa and 0.115 dpa) are shown and also the doses where subfigures b-d are placed are displayed. In subfigure b a Frank loop (dark blue) starts to grow on a Shockley partial chain at about 0.086 dpa. The graph shows a very turbulent defect evolution at this dose. In subfigure c at about 0.097 dpa the Shockley partial chain has been absorbed halfway. We see a drop of about 200 defects in the graph around this dose. In subfigure d after about 0.1 dpa the Frank loop has absorbed the whole Shockley partial chain. The defect count starts rising again in the graph but with a much milder variation. The meaning of the lines are the same as in Fig. 1.

3.3. Dislocation Mobility

The dynamics of the evolution of dislocation structures during the irradiation process highlights the necessity of good understanding of the mobility of dislocations in the studied materials. In this subsection, we systematically study the mobility of edge dislocations in all investigated alloys by analyzing the velocity of dislocations as a function of shear stress. In Fig. 8, the results for NiCo and NiCoFe are compared with those from Ref. 13, obtained for Ni, NiFe and NiCoCr. The results presented in the figure are the average velocity of the dislocations after they reached a steady movement. Previously it was observed significant differences in edge dislocation mobility for the three materials, Ni, NiFe and NiCoCr. These are ordered according to the mobility of dislocations from fastest to slowest. Adding two new alloys, we see that NiCo shows mobility similar to pure Ni, and NiCoFe shows very similar result to NiFe. The highest mobility is seen for Ni and NiCo, and the dislocations in these materials reach steady movement at low stresses, these two alloys also show the most accumulated damage. NiFe and NiCoFe show lower mobility, they also need higher stress for steady movement. Moreover, both of them show very similar accumulated damage, which is lower than in Ni and NiCo. This is especially clear in the large simulation cell. NiCoCr showed a very high onset stress for steady state movement and also a lower mobility than the other materials, and NiCoCr also showed the least accumulated damage. In Fig. 9, the saturated defect amount in the different alloys are plotted against their corresponding dislocation mobilities. The mobilities were obtained by fitting a linear regression to the linear part of the Fig. 8. This figure clearly indicates that there is a correlation between the edge dislocation mobility and the accumulated defect amount.

In the previous study [13], it was seen that the edge dislocation started to move steadily in Ni even at the lowest investigated stress of roughly 6 MPa. The NiCo and the NiCoFe alloys did show a higher stress needed for steady movement, and also some differences between the different cases for the same material. The NiCo alloy resulted in an onset stress for steady movement. In this case, two out of three dislocations did move at 24 MPa, while all three started to move steadily only at 35 MPa. The NiCoFe alloy, on the other hand, resulted in higher onset stress, with one out of three dislocations starting to move steadily at 58 MPa and all three at 70 MPa. The result of NiCoFe is very close to that of the NiFe alloy. At the higher stresses, we see that the NiCo alloy plateaus at a level a little lower than that of elemental Ni. The NiCoFe alloy, on the other hand, shows a similar trend as the NiFe alloy.

In the following, we qualitatively investigate the stacking fault energy (SFE) in the different materials. For this, we studied the separation of the two partials of the pure edge dislocation. The distance between the two partials is inversely proportional to the SFE in the material [32]. The separation d can be estimated as

$$d = \frac{Gb^2}{4\pi\gamma}, \tag{1}$$

where G is the shear modulus, b the length of the Burgers vector and γ the SFE. Snapshots of the edge dislocations in the different materials at 300 K can be seen in the supplementary. Now, ananlyzing this parameter d for all studied materials and assuming that the shear modulus does not change, we can see that Ni shows the highest SFE, NiFe a bit lower SFE and the NiCo, NiCoCr and NiCoFe the lowest SFE. In the alloys, the separation is heavily dependent on the local environment, and the exact values cannot be obtained in this manner. The results, however, will show that the SFE of the materials will not explain the formation of SFTs alone. It is known that SFTs are formed usually in materials with a low SFE [32], however, in our results we do not observe a strong correlation between low SFE and higher probability of formation of SFTs. Most likely the explanation of The formation of large numbers of SFTs in Ni and NiCo can be due to a lower vacancy migration barrier than in the other alloys, which is one of the mechanism of growth of SFTs.

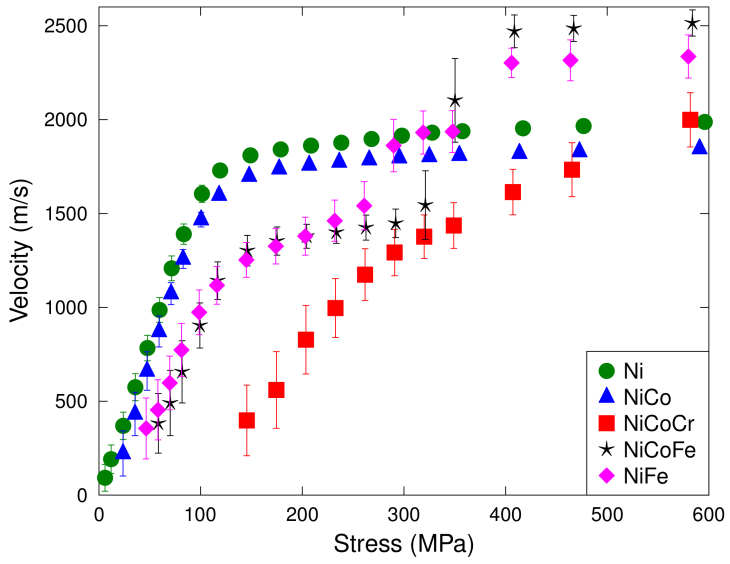

Figure 8: Edge dislocation velocity as a function of stress in different materials.

4. Conclusions

In this article, we have in detail studied the defect and dislocation evolution in different sized cells of five different equiatomic multicomponent alloys, in massively overlapping cascades by computational means. We found that the

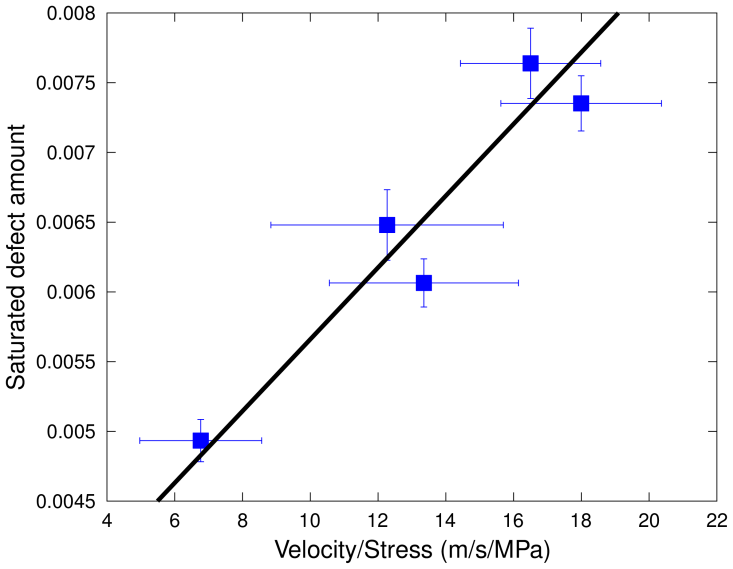

Figure 9: The saturated defect level as a function of dislocation mobility, for all investigated alloys. The line is a linear fit to the data points to guide the eye.

different alloys reacted differently to irradiation, and differently compared to elemental Ni. The previous studies showed that addition of Fe or Co and Cr, improved the response to irradiation, as a decrease in accumulated defects in the alloys. The same trend was even more clearly seen in our larger simulation cells. The investigation of addition of Co or Co and Fe showed some differences to the previous result. We found that addition of an element is not enough to obtain better radiation response in form of lower level of accumulated defects, as the NiCo alloy showed similar defect buildup evolution as elemental Ni. The NiCoFe alloy showed a very similar behaviour to the two component NiFe, which indicates that already 33 % of Fe is enough to obtain a better response, in the investigated crystal structure. The NiCoCr alloy shows a superior response to irradiation to all other studied alloys, clearly seen in the comparison of the large simulation cells. A comparison of the ternary alloys, NiCoFe and NiCoCr, also show the effect of a choice of alloying element. In our simulations we saw that the NiCoCr alloy showed a much stronger decrease of damage level than the NiCoFe alloy. The new results show the importance of the choice of alloying elements, as the complexity is not the only factor affecting the damage buildup in the materials.

Previously it was seen that the dislocation mobility is a key factor that is

responsible to this defect accumulation reduction [5]. A difference in the mobility of edge dislocations was also seen, if the alloys are compared to elemental Ni [13]. In this article, we see that NiCo shows a very similar mobility as the elemental Ni, which can explain the similar defect buildup. Also the mobility of edge dislocations in NiCoFe shows a very similar mobility and the onset stress for steady movement as NiFe, and also their response to irradiation is very similar. The mobility is much lower and the onset stress required is much higher for NiCoCr, which is the alloy that shows the lowest level of accumulated defects. If the saturated defect level of the different samples are plotted against their corresponding edge dislocation mobility (see Fig. 9), we can clearly see a correlation between the damage level and the dislocation mobility.

In addition to our defect evolution analysis, we have made a qualitative, and to some extent, quantitative analysis of the different dislocation evolutions in our materials. We noticed that elemental Ni shares similar dislocation evolution behavior with NiCo, while the dislocation evolution behaves similarly in the remaining alloys, except for one case of NiCoFe that resulted in similar absorption events as Ni and NiCo. We showed that one can correlate, to some extent, defect evolution with dislocation structures in Ni and NiCo.

5. Acknowledgements

This research was funded by the Academy of Finland project SIRDAME (grant no. 259886). We thank the IT Center for Science, CSC, for granted computational resources. This work has been carried out within the framework of the EUROfusion Consortium and has received funding from the Euratom research and training programme 2014 - 2018 under grant agreement No 633053. The views and opinions expressed herein do not necessarily reflect those of the European Commission.

[1] B. Cantor, I. Chang, P. Knight, A. Vincent, Microstructural development in equiatomic multicomponent alloys, Mat. Sci. and Eng. A 375–377 (2004) 213 – 218.

[2] J.-W. Yeh, S.-K. Chen, S.-J. Lin, J.-Y. Gan, T.-S. Chin, T.-T. Shun, C.-H. Tsau, S.-Y. Chang, Nanostructured high-entropy alloys with multiple principal elements: Novel alloy design concepts and outcomes, Adv. Eng. Mat. 6 (5) (2004) 299–303.

[3] B. Gludovatz, A. Hohenwarter, D. Catoor, E. H. Chang, E. P. George, R. O. Ritchie, A fracture-resistant high-entropy alloy for cryogenic applications, Science 345 (6201) (2014) 1153–1158.

[4] M.-H. Tsai, J.-W. Yeh, High-entropy alloys: A critical review, Mat. Res. Lett. 2 (3) (2014) 107–123.

[5] F. Granberg, K. Nordlund, M. W. Ullah, K. Jin, C. Lu, H. Bei, L. M. Wang, F. Djurabekova, W. J. Weber, Y. Zhang, Mechanism of radiation

damage reduction in equiatomic multicomponent single phase alloys, Phys. Rev. Lett. 116 (13).

[6] O. N. Senkov, G. B. Wilks, D. B. Miracle, C. P. Chuang, P. K. Liaw, Refractory high-entropy alloys, Intermetallics 18 (9) (2010) 1758–1765.

[7] O. N. Senkov, G. B. Wilks, J. M. Scott, D. B. Miracle, Mechanical properties of $Nb_{25}Mo_{25}Ta_{25}W_{25}$ and $V_{20}Nb_{20}Mo_{20}Ta_{20}W_{20}$ refractory high entropy alloys, Intermetallics 19 (5) (2011) 698–706.

[8] Z. Wu, H. Bei, G. M. Pharr, E. P. George, Temperature dependence of the mechanical properties of equiatomic solid solution alloys with face-centered cubic crystal structures, Acta Mat. 81 (2014) 428–441.

[9] B. Gludovatz, A. Hohenwarter, K. V. S. Thurston, H. Bei, Z. Wu, E. P. George, R. O. Ritchie, Exceptional damage-tolerance of a medium-entropy alloy CrCoNi at cryogenic temperatures, Nat. Comm. 7.

[10] Y. Wei, Y. Li, L. Zhu, Y. Liu, X. Lei, G. Wang, Y. Wu, Z. Mi, J. Liu, H. Wang, H. Gao, Evading the strength- ductility trade-off dilemma in steel through gradient hierarchical nanotwins, Nat. Comm. 5.

[11] Y. Zhang, M. Stocks G., K. Jin, C. Lu, H. Bei, B. C. Sales, L. Wang, L. K. Beland, R. E. Stoller, G. D. Samolyuk, M. Caro, A. Caro, W. J. Weber, Influence of chemical disorder on energy dissipation and defect evolution in concentrated solid solution alloys, Nat. Comm. 6.

[12] Y. Zhang, K. Jin, H. Xue, C. Lu, R. J. Olsen, L. K. Beland, M. W. Ullah, S. Zhao, H. Bei, D. S. Aidhy, G. D. Samolyuk, L. Wang, M. Caro, A. Caro, G. M. Stocks, B. C. Larson, I. M. Robertson, A. A. Correa, W. J. Weber, Influence of chemical disorder on energy dissipation and defect evolution in advanced alloys, J. of Mat. Res. 31 (16) (2016) 2363–2375.

[13] F. Granberg, F. Djurabekova, E. Levo, K. Nordlund, Damage buildup and edge dislocation mobility in equiatomic multicomponent alloys, Nucl. Instr. Meth. Phys. Res. B. 393 (2017) 114 – 117.

[14] K. Nordlund, L. Wei, Y. Zhong, R. S. Averback, Role of electron-phonon coupling on collision cascade development in Ni, Pd and Pt, Phys. Rev. B (Rapid Comm.) 57 (1998) 13965–13968.

[15] A. E. Sand, S. L. Dudarev, K. Nordlund, High energy collision cascades in tungsten: dislocation loops structure and clustering scaling laws, EPL 103 (2013) 46003.

[16] A. E. Stuchbery, E. Bezakova, Thermal-spike lifetime from picosecond-duration preequilibrium effects in hyperfine magnetic fields following ion implantation, Phys. Rev. Lett. 82 (18) (1999) 3637.

[17] K. Nordlund, S. J. Zinkle, T. Suzudo, R. S. Averback, A. Meinander, F. Granberg, L. Malerba, R. Stoller, F. Banhart, B. Weber, F. Willaime, S. Dudarev, D. Simeone, Primary radiation damage in materials: Review of current understanding and proposed new standard displacement damage model to incorporate in-cascade mixing and defect production efficiency effects, OECD Nucl. Energy Ag., Paris, France, 2015.

[18] K. Nordlund, M. Ghaly, R. S. Averback, M. Caturla, T. Diaz de la Rubia, J. Tarus, Defect production in collision cascades in elemental semiconductors and FCC metals, Phys. Rev. B 57 (13) (1998) 7556–7570.

[19] K. Nordlund, J. Keinonen, M. Ghaly, R. S. Averback, Coherent displacement of atoms during ion irradiation, Nature 398 (6722) (1999) 49–51.

[20] X. W. Zhou, R. A. Johnson, H. N. G. Wadley, Misfit-energy-increasing dislocations in vapor-deposited CoFe/NiFe multilayers, Phys. Rev. B 69 (2004) 144113.

[21] Z. Lin, R. A. Johnson, L. V. Zhigilei, Computational study of the generation of crystal defects in a BCC metal target irradiated by short laser pulses, Phys. Rev. B 77 (214108).

[22] J. F. Ziegler, SRIM-2013 software package, available online at *http://www.srim.org*.

[23] J. F. Ziegler, J. P. Biersack, U. Littmark, The Stopping and Range of Ions in Matter, Pergamon, New York, 1985.

[24] H. J. C. Berendsen, J. P. M. Postma, W. F. van Gunsteren, A. DiNola, J. R. Haak, Molecular dynamics with coupling to external bath, J. Chem. Phys. 81 (8) (1984) 3684.

[25] A. Stukowski, Visualization and analysis of atomistic simulation data with OVITO–the open visualization tool, Modell. and Simul. in Mat. Sci. and Eng. 18 (1) (2010) 015012.

[26] A. Stukowski, V. V. Bulatov, A. Arsenlis, Automated identification and indexing of dislocations in crystal interfaces, Modell. and Simul. in Mat. Sci. and Eng. 20 (8) (2012) 085007.

[27] C. Lu, K. Jin, L. Béland, F. Zhang, T. Yang, L. Qiao, Y. Zhang, H. Bei, H. Christen, R. Stoller, L. Wang, Direct observation of defect range and evolution in ion-irradiated single crystalline Ni and Ni binary alloys, Sci. Rep. 6.

[28] K. Vörtler, N. Juslin, G. Bonny, L. Malerba, K. Nordlund, The effect of prolonged irradiation on defect production and ordering in fe–cr and fe–ni alloys, J. Phys.: Condens. Mat. 23 (35) (2011) 355007.

[29] R. S. Averback, T. Diaz de la Rubia, Displacement damage in irradiated metals and semiconductors, in: H. Ehrenfest, F. Spaepen (Eds.), Solid State Physics, Vol. 51, Academic Press, New York, 1998, pp. 281–402.

[30] S. Zhang, K. Nordlund, F. Djurabekova, F. Granberg, Y. Zhang, T. Wang, Radiation damage buildup by athermal defect reactions in nickel and concentrated nickel alloys, Mat. Res. Lett. Accepted for publication. doi:10.1080/21663831.2017.1311284.

[31] R. Schäublin, Z. Yao, N. Baluc, M. Victoria, Irradiation-induced stacking fault tetrahedra in fcc metals, Phil. Mag. 85 (4-7) (2005) 769–777.

[32] D. Hull, D. J. Bacon, Introduction to dislocations, 4th Edition, Butterworth-Heinemann, Oxford, 2001.